

# Co-Axial Gyro-Spinning of PCL/PVA/HA Core-Sheath Fibrous Scaffolds for Bone Tissue Engineering

Suntharavathanan Mahalingam, Cem Bayram, Merve Gultekinoglu, Kezban Ulubayram, Shervanthi Homer-Vanniasinkam, and Mohan Edirisinghe\*

The present study aspires towards fabricating core-sheath fibrous scaffolds by state-of-the-art pressurized gyration for bone tissue engineering applications. The core-sheath fibers comprising dual-phase poly- $\epsilon$ -caprolactone (PCL) core and polyvinyl alcohol (PVA) sheath are fabricated using a novel “co-axial” pressurized gyration method. Hydroxyapatite (HA) nanocrystals are embedded in the sheath of the fabricated scaffolds to improve the performance for application as a bone tissue regeneration material. The diameter of the fabricated fiber is  $3.97 \pm 1.31 \mu\text{m}$  for PCL-PVA/3%HA while pure PCL-PVA with no HA loading gives  $3.03 \pm 0.45 \mu\text{m}$ . Bead-free fiber morphology is ascertained for all sample groups. The chemistry, water contact angle and swelling behavior measurements of the fabricated core-sheath fibrous scaffolds indicate the suitability of the structures in cellular activities. Saos-2 bone osteosarcoma cells are employed to determine the biocompatibility of the scaffolds, wherein none of the scaffolds possess any cytotoxicity effect, while cell proliferation of 94% is obtained for PCL-PVA/5%HA fibers. The alkaline phosphatase activity results suggest the osteogenic activities on the scaffolds begin earlier than day 7. Overall, adaptations of co-axial pressurized gyration provides the flexibility to embed or encapsulate bioactive substances in core-sheath fiber assemblies and is a promising strategy for bone healing.

## 1. Introduction

Bone is an indispensable part of the human musculoskeletal system that attaches muscles, ligaments, and tendons for locomotive action.<sup>[1]</sup> Bone comprises a highly complex organic-inorganic architecture and as a tissue consists of collagen, calcium phosphate, and multiple cell types.<sup>[2]</sup> Bone has the capacity to regenerate and heal small defects, for example, minor fractures; however, large defects and major fractures require bone grafting and/or fixation, to aid full recovery.<sup>[3]</sup> Large bone defects require bone fixation through autografts or allografts for complete healing to be achieved.<sup>[4,5]</sup> The autografts and allografts techniques are considered to be a gold-standard treatment for large bone defects but they suffer from limitations such as multiple surgeries, potential morbidity, immunogenic responses, infection, and pathogen transmissions.<sup>[6]</sup> Bone tissue engineering emerged as an alternative approach and efficient methodology to heal, repair, and reconstruct large bone defects and tissues, and has generated substantial


development in bone-regeneration thus eliminating the drawbacks pertaining to autografts and allografts.<sup>[7-9]</sup>

Bone tissue engineering involves applying the principles of engineering and life sciences toward the development of bone substitute that can restore, maintain, or enhance the function of the bone tissue.<sup>[10]</sup> The success of bone tissue engineering relies on the selection of materials, material design, and scalable fabrication techniques that enable the formation of tissue construct at multiple length scales.<sup>[11]</sup> The material used in bone tissue engineering is often assembled in the form of a scaffold which provides a template and extracellular environment for cell seeding, cell attachment and facilitates cellular activities for bone growth.<sup>[12-14]</sup> These scaffolds must possess certain characteristics of the native extracellular matrix (ECM) of tissues incorporating design features such as bioactivity, biocompatibility, mechanical and degradable properties, material composition and surface topology for physical, chemical, and biological cues to accelerate the healing process.<sup>[11,15]</sup> Collagen coated biomimetic tofu scaffolds, F127-DA/nano-CaCO<sub>3</sub> composite hydrogels and arginine-poly (ester amide)-hyaluronic acid bioactive hydrogels are very recent scaffold examples which are tailored for bone tissue engineering.<sup>[16-18]</sup>

S. Mahalingam, S. Homer-Vanniasinkam, M. Edirisinghe  
Department of Mechanical Engineering  
University College London  
London WC1E 7JE, UK  
E-mail: m.edirisinghe@ucl.ac.uk

C. Bayram, K. Ulubayram  
Department of Nanotechnology and Nanomedicine  
Hacettepe University  
Ankara 06800, Turkey

M. Gultekinoglu, K. Ulubayram  
Department of Basic Pharmaceutical Sciences, Hacettepe University  
Ankara 06100, Turkey

 The ORCID identification number(s) for the author(s) of this article can be found under <https://doi.org/10.1002/mabi.202100177>

© 2021 The Authors. Macromolecular Bioscience published by Wiley-VCH GmbH. This is an open access article under the terms of the Creative Commons Attribution License, which permits use, distribution and reproduction in any medium, provided the original work is properly cited.

DOI: 10.1002/mabi.202100177

Core-sheath fibrous scaffolds made with two different polymer phases provide the relevant properties for a tissue engineering scaffold, making it attractive for such applications.<sup>[19]</sup> In addition, combining these scaffolds with particulate material like nano-hydroxyapatite (nHA) enhances the osteoconductive property which is a prerequisite for new bone formation.<sup>[20]</sup> Further, the osteo-inductive property could be tuned into these scaffolds by embedding and encapsulating growth factors like bone morphogenic protein (BMPs) and connective tissue growth factors (CTGFs).<sup>[21]</sup> The vascularization potential is considered to be another crucial factor for successful bone repair that could be achieved by incorporating vascular endothelial growth factor (VEGF) in the compartmentalized core-sheath fibrous scaffolds.<sup>[22]</sup> These scaffolds could be utilized as orthopaedic implants to promote osseointegration and prevent bacterial colonization by sustained release of antibiotics within the fibers.<sup>[23]</sup> Moreover, the controlled release of adenosine enclosed in the sheath structure facilitates the osteogenic differentiation of bone mesenchymal progenitor cells (BMSCs) and promotes bone regeneration.<sup>[24]</sup>

Poly- $\epsilon$ -caprolactone (PCL) and polyvinyl alcohol (PVA) are two principal synthetic polymers used in tissue engineering applications owing to their biodegradability and biocompatibility.<sup>[9,25,26]</sup> PCL is a highly hydrophobic biopolymer which exhibits excellent mechanical properties, however it lacks cell recognition sites and shows reduced cellular attachment.<sup>[27–30]</sup> PVA is hydrophilic and has a greater affinity for cell seeding and cell adhesion.<sup>[21,31]</sup> Hydroxyapatite, an inorganic substance which is an essential component of bone, demonstrates superior biocompatibility and, is osteoconductive; due to its osteointegration properties, it is used in bone tissue engineering and bone implants.<sup>[32–36]</sup> The construction of a core-sheath fibrous scaffold with a combination of PCL, PVA and HA, as attempted in this work, provides a viable platform to potentially repair bone defects by harnessing the unique properties of each compound.

Co-axial pressurised gyration, which can also be called core-sheath pressurised gyration, is a novel fiber spinning technique that has been shown to produce core-sheath fibers with two different polymer phases,<sup>[37,38]</sup> and can be complementary to electrospinning.<sup>[39]</sup> In this technique, the polymer solutions are loaded into a custom-built spinning device and forcibly extruded through concentric nozzles by the action of rotation and pressure.<sup>[37]</sup> The pressurised gyration technique has distinct advantages over fiber production techniques such as electrospinning or wet-spinning. The most important advantages are that there is no need for an electric field and there are no restrictions on solvents due to solubility or vapor pressure. Pressurised gyration is a superior technique for the production of polymeric nanofibers on a large scale with a single step process. Additionally, room temperature fiber characteristics can be varied easily by manipulating applied pressure, rotating speed and/or polymer solution (concentration, viscosity, surface tension) properties. A wide variety of polymer-solvent combinations could be used to make multicomponent fibers by pressurised gyration with the flexibility to functionalize the fibers by the addition of nanoparticles, peptides and drugs sought after using other methods.<sup>[40–42]</sup> In this study, we aim to: (i) prepare PCL/PVA core-sheath fibers (ii) perform solution blending on the sheath component to deliver biological cues for tissue regeneration by having

HA nanoparticles embedded in PVA (iii) evaluate these fibers for bone tissue engineering.

Most methods of fiber forming do not consider the fact that the functional properties are only necessary in a thin surface layer. This method of core-sheath pressurised gyration, easily amenable to scale up and economical mass production/manufacturing delivers exactly that. So strong core and thin sheath fibers are generated and here the sheath is filled with bioactive hydroxyapatite to entice fibroblast activity at the surface, in this specific application to benefit bone tissue engineering. However, this is a platform technology which can be used in any such biomedical engineering functional scenario such as very topical (pandemic) antimicrobial surface activity.

## 2. Results and Discussion

### 2.1. Properties of Spinning Dopes

The spin ability of the spinning dopes to form filament or fiber and the morphology of the fabricated fibers greatly depends on solution properties viscosity and surface tension. **Figure 1A** depicts the apparent viscosities of PVA and HA containing PVA solutions as a function of shear rate. In the measured range, the PVA solution exhibits Newtonian fluid behaviour. The PVA/HA solutions display non-Newtonian flow and shear-thinning effect at the higher shear rates. The solid or volume fractions of HA particles in PVA solutions had a noticeable change in the apparent viscosities at a shear rate of  $1.32 \text{ s}^{-1}$  (**Figure 1B**). The PVA/HA suspension viscosity increases with increasing solid fractions. The viscosity of the PCL solution obtained at a shear rate of  $1.32 \text{ s}^{-1}$  is  $3299 \text{ mPa s}$ . It is two orders of magnitude higher than the pure PVA and PVA/HA suspensions. The viscous properties and the viscoelastic nature of the liquid jets are fundamental features of jet dynamics, the solidification and therefore the fiber formation processes.<sup>[43]</sup> The capillary forces are another parameter that governs dripping, jetting, and the stability of the jets before eventual break-up or hardening to form droplets or fibers.<sup>[44]</sup>

**Table 1** shows the surface tensions of PVA, PCL, and PVA/HA suspensions obtained. The surface tension values of pure PVA and PVA/HA suspensions are significantly higher than that of the PCL solution. The surface tension of pure PVA and PVA/HA suspensions are not very disparate indicating the solid fraction had no impact on the values obtained.

### 2.2. Fabrication of PCL–PVA/HA Core-Sheath Fibers

Co-axial gyro-spinning concurrently utilizes centrifugal force and pressure drop to pull the solid core-sheath fibers from the spinning dopes that undergo chemical changes (in the form of solvent evaporation) and physical changes (in the form of mechanical stretching). It is a versatile, robust and industrially scalable process to generate high-performance functional polymer fibers from a wide variety of polymers and solvents.<sup>[19,37,38]</sup> As mentioned before, to re-emphasise PVA/HA suspension viscosity increases with increasing solid fractions. Additionally, the solid or volume fractions of HA particles in PVA solutions had

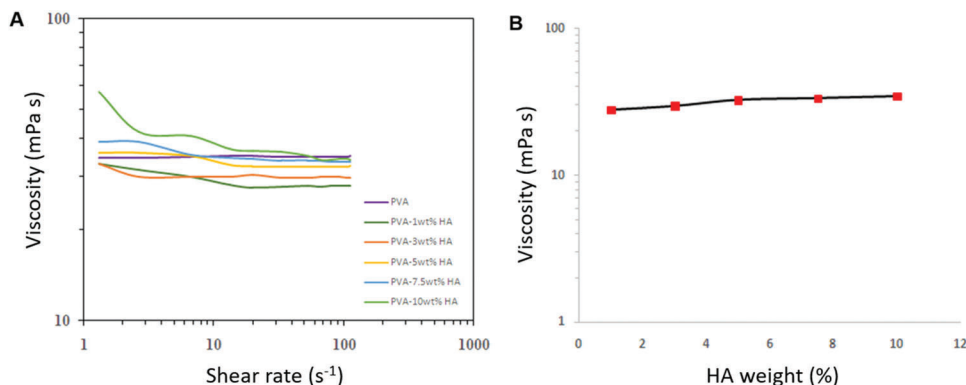


**Figure 1.** A) Viscosity of PVA and PVA/HA solutions as a function of shear rate. B) The viscosity of PVA/HA suspension as a function of solid fraction.

**Table 1.** The surface tension values of spinning dopes at room temperature.

Solution/suspension	Surface tension [mN m <sup>-1</sup> ]
PCL	27.6
PVA	53.5
PVA/1%HA	53.8
PVA/3%HA	52.5
PVA/5%HA	52.7
PVA/7.5%HA	52.1
PVA/10%HA	52.3

a noticeable change in the apparent viscosities at a shear rate of  $1.32 \text{ s}^{-1}$  (Figure 1B). The viscosity of the PCL solution obtained at a shear rate of  $1.32 \text{ s}^{-1}$  is  $3299 \text{ mPa s}$ . It is two orders of magnitude higher than the pure PVA and PVA/HA suspensions. The viscous properties and the viscoelastic nature of the liquid jets are fundamental features of the fiber formation processes. The capillary forces are another parameter that govern the eventual break-up or hardening to form droplets or fibers. The surface tension values of pure PVA and PVA/HA suspensions are significantly higher than that of the PCL solution. The surface tension of pure PVA and PVA/HA suspensions are not very disparate indicating the solid fraction had no impact on the values obtained. The mechanism involved in fabricating core-sheath fibers from co-axial gyro-spinning is more complex, principally, external energy must be applied to the polymer solutions to extrude the filaments or fibers. The focused phase (core) is coaxially injected into a second immiscible focusing phase (sheath) and forced by pressure through an orifice. A stable jet will be obtained when the focused liquid and focusing liquid are fed at the same rate.<sup>[45]</sup> Initially, a core-sheath polymer droplet forms at the tip of the nozzle due to capillary or surface tension force. Thereafter, the droplet elongates due to stress generated mainly by the spinning action of the vessel and the high-velocity gas-flow (Figure 2A). The high-velocity gas-flow deforms the droplet into a conical shape and creates a pressure drop  $P_2$  along with the flow of the compressed gas as shown in Figure 2B. Here,  $P_2 < P_{\text{atm}} < P_1$ . The pressure drop creates a partial vacuum both inside the inner nozzle and the outer nozzle which ultimately attracts the respective polymer solutions to form core-sheath fibers.<sup>[40]</sup>

### 2.3. Structural Verification of PCL–PVA/HA Core-Sheath Fibers

To confirm the core-sheath structure formation in co-axial gyro-spinning, fluorescent dyes were incorporated in the respective spinning dopes and observed under the optical microscope. Figure 2C shows the optical micrograph of the PCL–PVA/HA core-sheath fiber obtained at  $6000 \text{ rpm}$  and  $1 \times 10^5 \text{ Pa}$  working pressure. As shown in Figure 2C, distinctive fluorescence patterns at the inner (PCL) and outer (PVA) layers confirm the presence and location of both polymeric materials using this method. The incorporation of HA nanoparticles on the surface of the PVA sheath fiber is verified by backscattered scanning electron micrograph as shown in the inset of Figure 2C. PCL–PVA/HA fiber surface elemental analysis was also performed by EDX analysis and the spectrum is shown in Figure 2D.

### 2.4. Morphology and Fiber Diameter Analysis

Typical morphologies of the manufactured PCL-PVA/HA fibers with various HA content are represented in the scanning electron micrographs depicted in Figure 3-i. Both pure PCL–PVA fibers with no HA content and PCL–PVA fibers with varying HA show uniform, bead-free fiber morphology. The surface of the fibers appears quite rough with no visible pores. The bead-free fiber morphologies are indicative of suppression of capillary instability and the dominant viscoelasticity of the polymer solutions during fiber spinning.<sup>[46–48]</sup>

Figure 3-ii represents the fiber diameter analysis of the PCL–PVA/HA core-sheath fibers obtained at  $6000 \text{ rpm}$  and  $1 \times 10^5 \text{ Pa}$  working pressure. The pure PCL–PVA core-sheath fibers with no HA content provided a mean fiber diameter (FD) of  $3.03 \mu\text{m}$  with a standard deviation (SD) of  $0.45 \mu\text{m}$ . Generally, the mean fiber diameter is increased with the HA concentration. The increase of fiber diameter with a HA concentration is due to the increase of viscosity of the polymer solutions. The highest fiber diameter is obtained for PCL-PVA/3%HA with a mean of  $3.97 \mu\text{m}$  and a standard deviation of  $1.31 \mu\text{m}$ . For higher concentrations of HA ( $>5\%$ ), a noticeable decrease in fiber diameter is observed owing to coalesce of HA particles during fiber spinning. The coefficient of variation (CV) of fiber diameter is calculated by  $\text{SD}/\text{FD}$ . The uniformity (smoothness) of the fibers could be demarcated with the coefficient of variation, where  $\text{SD}/\text{FD} < 0.3$

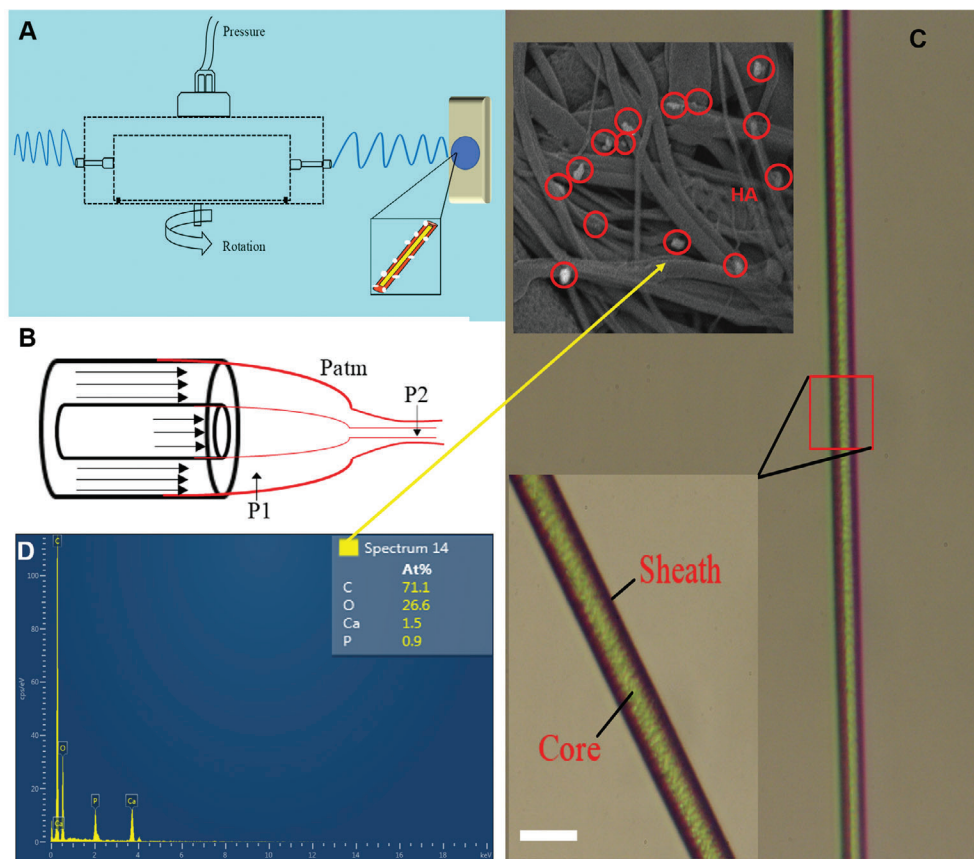


**Figure 2.** A) Experimental setup of the co-axial pressurised gyration device to generate PCL-PVA/HA core-sheath fibers, B) Graphical representation of core-sheath fiber formation using co-axial gyro-spinning, C) Optical micrograph of the formed PCL-PVA/HA core-sheath fiber. The upper inset shows the backscattered scanning electron micrograph of the PCL-PVA/HA core-sheath fiber and the lower inset shows the magnified optical micrograph representing a scale bar 20  $\mu\text{m}$ , D) EDX spectrum data of PCL-PVA/HA fiber surface elemental analysis.

indicates smooth fibers and  $SD/FD > 0.3$  indicates non-uniform fibers.<sup>[49]</sup> The smooth fibers are obtained for PCL-PVA/HA with no HA content, 1, 7.5, and 10% HA. The 3% and 5% HA content provided non-uniform fibers. This corresponds to the results obtained in the micrographs above.

## 2.5. FTIR Analysis

The FTIR spectra of PCL pellets, PVA powders, HA particles, and PCL-PVA/HA composite core-sheath fibers are presented in **Figure 4**. For PCL, the characteristic bands of  $\text{CH}_2$  asymmetric stretching at  $2952\text{ cm}^{-1}$  and symmetric stretching at  $2867\text{ cm}^{-1}$  are obtained. The ester carbonyl group ( $\text{C}=\text{O}$ ) peak is attained at  $1723\text{ cm}^{-1}$ . The peak  $1247\text{ cm}^{-1}$  belongs to  $\text{C}-\text{O}-\text{C}$  stretching while peak  $1170\text{ cm}^{-1}$  is associated with  $\text{C}-\text{O}$  stretching.<sup>[29,50]</sup> For PVA, the peak  $3280\text{ cm}^{-1}$  is due to  $-\text{OH}$  stretching,  $2917\text{ cm}^{-1}$  is assigned to  $\text{C}-\text{H}$  stretching, the peak at  $1425\text{ cm}^{-1}$  is associated with  $\text{CH}_2$  bending,  $1321\text{ cm}^{-1}$  is assigned to  $\text{C}-\text{H}$  deformation, the peaks  $1081$  and  $839\text{ cm}^{-1}$  are due to  $\text{C}-\text{O}$  stretching and  $\text{C}-\text{C}$  stretching, respectively.<sup>[51–53]</sup> In the case of HA particles, the peaks  $1454$  and  $1414\text{ cm}^{-1}$  are assigned to  $\text{C}-\text{O}$  stretching vibrations of  $\text{CO}_3^{2-}$ . The peak  $1034\text{ cm}^{-1}$  is tetrahedral  $\text{PO}_4^{3-}$

( $\nu_3$ ) mode and peaks  $605$  and  $566\text{ cm}^{-1}$  are from  $\text{PO}_4^{3-}$  ( $\nu_3$ ) mode.<sup>[54,55]</sup> The PCL-PVA/HA composite core-sheath fibers consist of all major peaks of the individual materials used to manufacture them confirming the core-sheath fiber formation and successful incorporation of HA particles on the surface of the fibers.

## 2.6. Water Contact Angle Measurement

Surface wettability is regarded as one of the desired material properties in tissue engineering and wound dressings, which may influence cell adhesion and migration in the spun fibers.<sup>[56]</sup> In addition, cellular proliferation is related to the hydrophilicity of the materials hence it may promote the rate of cellular proliferation.<sup>[57]</sup> Therefore, to assess the surface wettability and hydrophilicity of the spun fibers and the effect of HA on those properties, the water contact angle was measured and compared with pure PCL-PVA core-sheath fibers. A higher water contact angle shows a lower level of hydrophilicity, in general, the contact angle  $>90^\circ$  is considered to be hydrophobic and  $<90^\circ$  is hydrophilic.<sup>[58]</sup> **Figure 5A** displays the comparative plots of water contact angle measurements of PCL-PVA, PCL-PVA/1%HA,

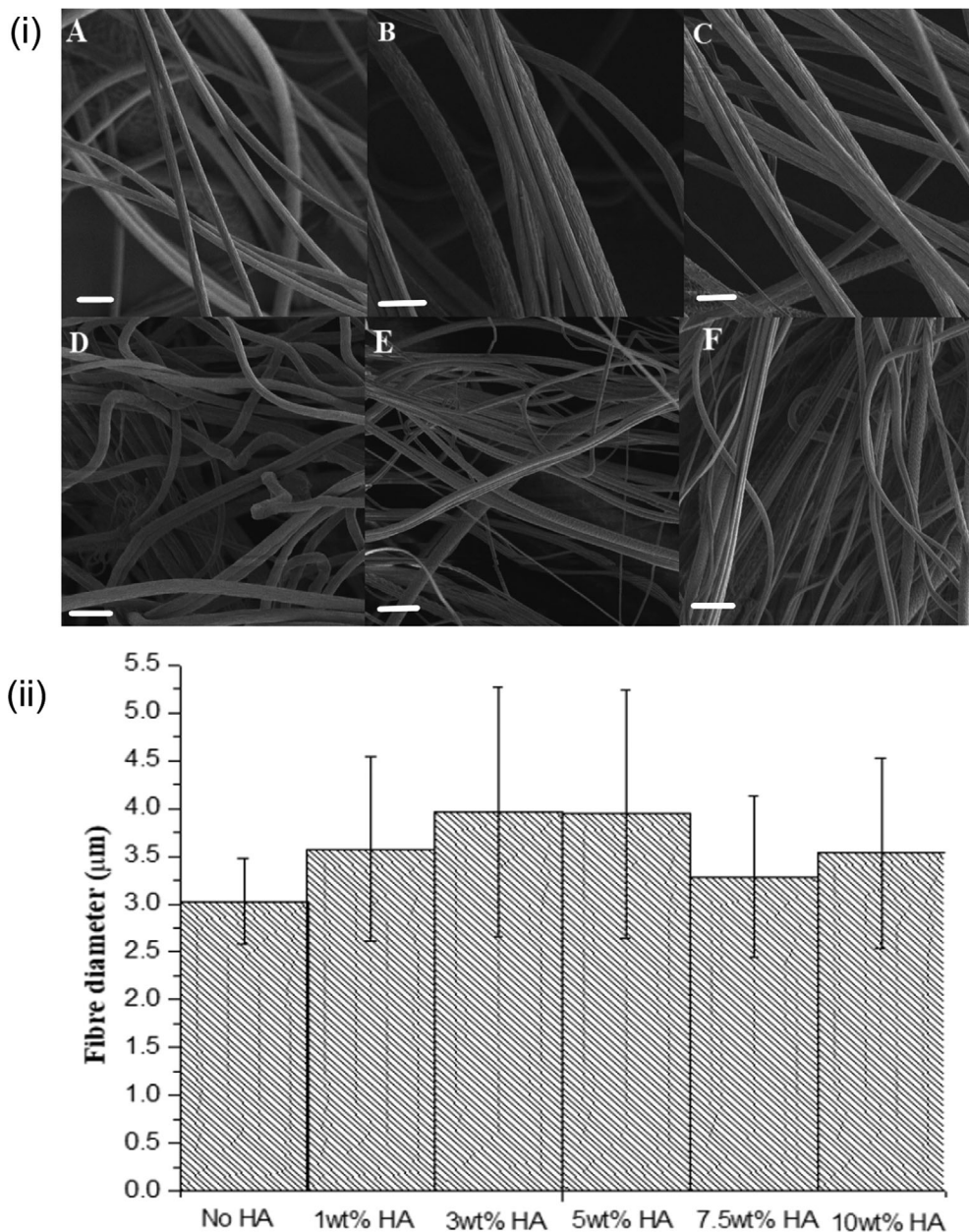


**Figure 3.** i) Scanning electron micrographs of the formed PCL–PVA/HA core-sheath fibers. A) no HA, B) 1% HA, C) 3% HA, D) 5% HA, E) 7.5% HA, and F) 10% HA. The scale bar represents 5 μm in the micrographs above, ii) Fiber diameter analysis of the formed PCL–PVA/HA core-sheath fibers.

PCL–PVA-5%HA, and PCL–PVA/10%HA fibers. The pure PCL–PVA fibers exhibited a water contact angle of  $59.2 \pm 5.5^\circ$  while PCL–PVA/1%HA showed  $41.7 \pm 6.9^\circ$  and PCL–PVA-5%HA gave  $40.5 \pm 6.5^\circ$ . The incorporation of HA dramatically decreased the water contact angle and abrupt increase of hydrophilicity of the fabricated core-sheath fibers. Interestingly, PCL–PVA/10%HA exhibited  $53.6 \pm 6.8^\circ$ , may be a result of the increasing roughness with chemical heterogeneity, obeying the Cassie–Baxter model. In this model, the increase in the contact angle can be related with the area fractions under the wetting phase.<sup>[59]</sup> Overall, all the samples were found to be hydrophilic which is beneficial to cell attachment and proliferation. Thus, the incorporation of HA on

the surface of the fibers enhances cell interaction than the pure PCL–PVA core-sheath fibers.<sup>[60]</sup>

### 2.7. Swelling Ratios of PCL–PVA/HA Core–Heath Fibrous Scaffolds

The swelling ratio represents the fluid intake capacity of the core-sheath fibrous scaffolds and plays a vital part in the adhesion and proliferation of bone cells. Figure 5B shows the swelling ratio of the fibrous scaffolds immersed in de-ionised water for up to 6 h at room temperature. The water absorption is

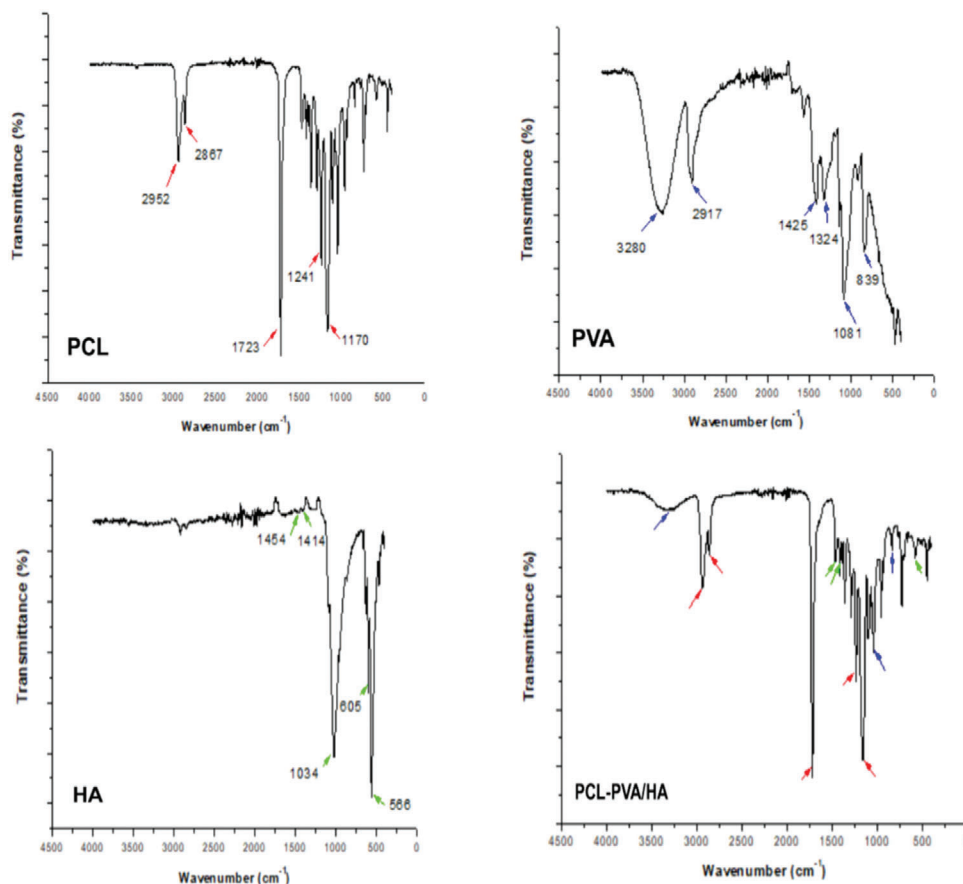


**Figure 4.** FTIR spectral analysis of materials and fibers; PCL, PVA, HA, and PCL–PVA/HA.

increased with immersion time for all the fibrous scaffolds. The pure PCL–PVA fibers showed the highest water intake capacity compared to PCL–PVA/HA fibers. Of the PCL–PVA/HA fibers, 1% HA loaded fibrous scaffolds exhibited greater affinity to water molecules than 5% and 10% HA loaded fibrous scaffolds. According to the increased inorganic HA content in the core-shell fibers, water swelling ratio decreased by the mass ratio of hydrophilic polymer reduction in the overall mass ratio. Increasing the HA loading in the fibers suppressed the swelling

ratio due to inhibition of diffusion of water molecules by HA particles.

### 2.8. In Vitro Biological Evaluation of PCL/PVA/HA Core-Sheath Fibers

Figure 6-i depicts the colorimetric MTT assay results for the quantitative evaluation of cytotoxicity, which indicates there is no

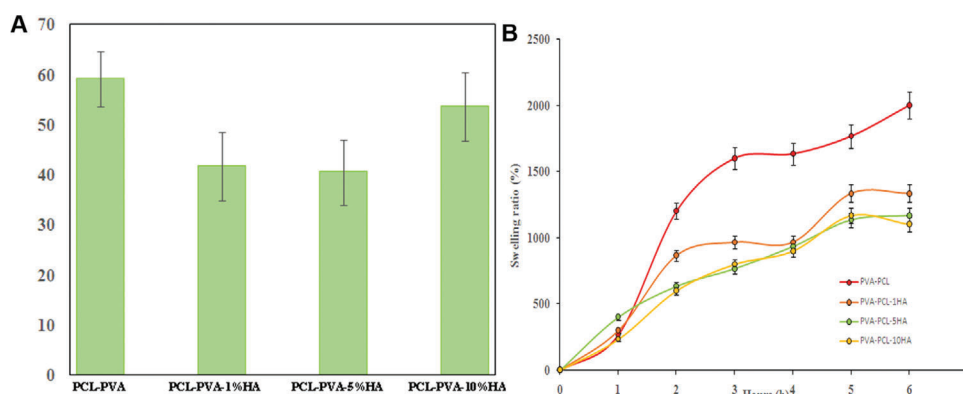


**Figure 5.** A) The comparative plots of water contact angle measurements of PCL–PVA, PCL–PVA/1%HA, PCL–PVA-5%HA and PCL–PVA/10%HA, B) The water absorption plots of PCL–PVA, PCL–PVA/1%HA, PCL–PVA-5%HA, and PCL–PVA/10%HA core-sheath fibrous scaffolds.

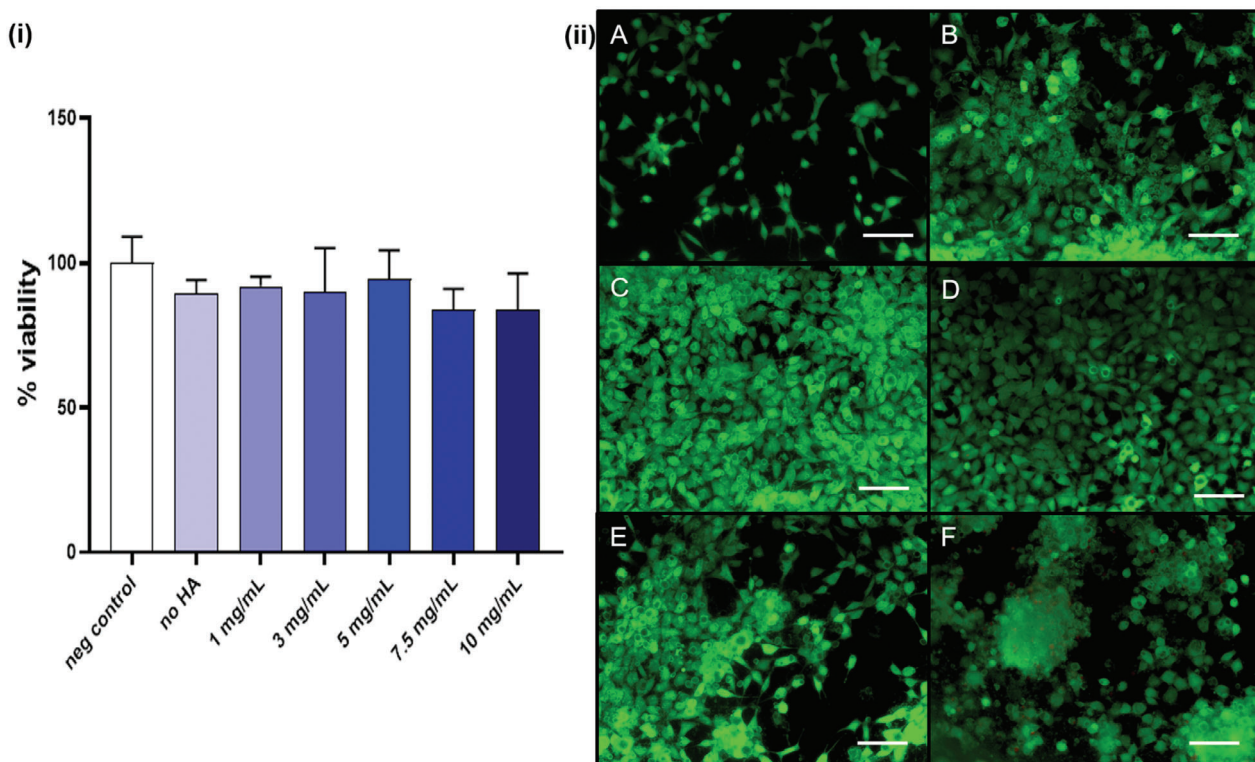


**Figure 6.** i) Cell viability analysis by colorimetric MTT Assay of PCL-PVA and PCL-PVA/HA fibrous scaffolds, ii) Fluorescence based LIVE/DEAD Assay ((A-F); 0, 1,3,5,7.5 and 10 mg mL<sup>-1</sup> HA, respectively) (scale bar = 100 μm).

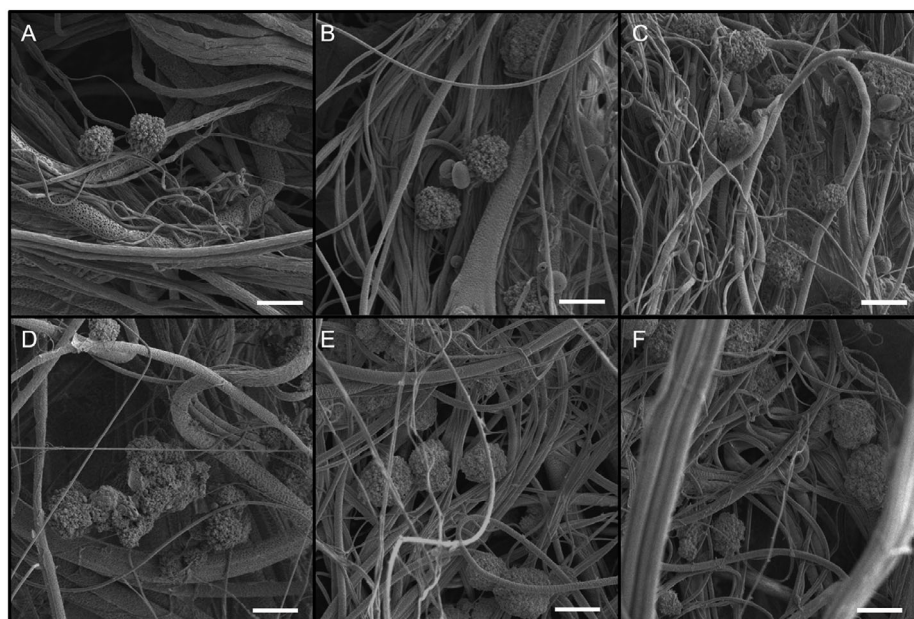


**Figure 7.** SEM images of SaOs-2 cells cultured on fibers on the 4th day ((A-F); 0, 1,3,5,7.5, and 10 mg mL<sup>-1</sup> HA, respectively) (scale bar = 20 μm).

statistical difference in cell viabilities. This result shows that the produced material has no toxic effects on mammalian cells in vitro. Cytotoxicity effects were also investigated by fluorescence dye-based live/dead assay to monitor the presence of dead cells,

however, no dead cells (red dye) were observed which corroborates the colorimetric MTT test (Figure 6-ii).

In addition to the fact that the samples were not cytotoxic, another remarkable finding noted on fluorescence imaging was that

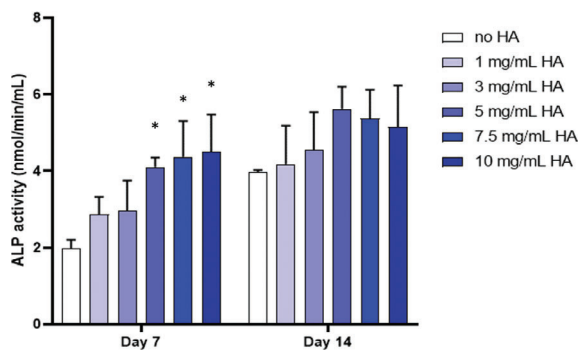


**Figure 8.** ALP activity assay results of SaOs-2 cells cultured on fiber samples on the 7th and 14th days. \* indicates the statistically significant difference of ALP activities with respect to the no HA group on day 7 ( $p < 0.05$ ).

the cells tend to generate clusters at high HA concentrations. The traces of HA crystals that originated from the sample extracts can also be noticed in Figure 6-ii (b–f) by revealing themselves as aggregated small grains. This cluster forming phenomenon can be attributed to the fact that the nHA play a functional role in integrin-mediated cell adhesion and signaling.<sup>[61]</sup> This feature is also noted on the SEM images where the SaOs- cells adhered more densely on some fibers where the sites of nHA crystals served as anchoring points (Figure 7).

The results of the ALP activity of the SaOs-2 cells cultured on the core-shell fibers on the 7th and the 14th days of the cell seeding are shown in Figure 8. The graph shows that the ALP activity increases with the HA wt% in polymer solutions, with respect to the fibers that do not contain HA. On day 14, there is no statistical difference amongst groups, however, on the 7th day, the higher levels of ALP activity for the sample groups containing HA 5% and above indicates that the osteogenic activity on these samples begins earlier.

The increase in ALP activity is generally attributed to early phase osteoblastic phenotype expression and osteogenic differentiation.<sup>[62,63]</sup> HA is the major inorganic constituent of the bone tissue and HA modification on the biomaterial surfaces causes increased osteogenic activity.<sup>[64–66]</sup>

### 3. Conclusion

The current study aimed to develop multi-material polymer fibers for bone tissue engineering using co-axial pressurised gyration. Using different processing conditions, micro-sized polymer fibrous scaffolds comprising a core region (PCL) and a sheath region (PVA/HA) were obtained with high cell affinity. The effects of HA concentration on the rheological properties and spinnability of the fibers were examined. The effect of the physical properties of the polymer solutions on the fiber morphology and fiber diameter have been elucidated. The core-sheath structure formation was demonstrated by optical microscopy images while scanning electron microscopy images characterized morphologies of the generated fibers. The bonding characteristics within the core-sheath fibers were confirmed by FTIR spectroscopy. The incorporation of HA nanoparticles on the surface of the fibers enhanced hydrophilicity. The water intake capacity of the scaffolds was increased with the immersion time. The in vitro cell culture studies

confirmed that the scaffolds were not cytotoxic, and that the HA nanocrystals acted as cell-binding sites. Furthermore, the alkaline phosphatase activity test demonstrated the osteogenic activity of the scaffolds and this activity increased in direct proportion to the HA nanoparticle concentration. This work pinpoints how the functional bioactivity of the scaffolds can be concentrated on the sheath (surface) while the core provides mechanical support, a very economical and effective way of harnessing the properties and benefits we require. A complimentary in vivo study together with appropriate degradation investigations of the binary polymer system contained in these core-sheath fibers is planned and early indications are that osteoblast response is very promising. These are essential components to bring these binary core-sheath bio-macromolecular polymeric fibers to actual application.

### 4. Experimental Section

**Materials:** Poly- $\epsilon$ -caprolactone (PCL,  $M_w = 80\,000$ ), polyvinyl alcohol (PVA,  $M_w = 50\,000$ ), hydroxyapatite (HA,  $M_w = 502.31$ ), and chloroform were purchased from Sigma-Aldrich (Dorset, UK). Dulbecco's modified eagle's medium (DMEM) and fetal bovine serum (FBS) were purchased from Bio-Ind (Israel). 3-(4,5-dimethylthiazol-2-yl)-2,5-diphenyltetrazolium bromide (MTT reagent) was from Merck (Germany). An alkaline phosphatase assay kit was ordered from Abcam (Cambridge, UK). Live/dead cell viability assay was purchased from Invitrogen (Paisley, UK). Saos-2 cell line was obtained from the Foot and Mouth Disease Institute (Ankara, Turkey).

**Preparation of Polymer Solutions:** A solution of 10% (w/w) of PCL was obtained by dissolving PCL pellets in chloroform. The obtained solution was magnetically stirred for 24 h at room temperature (20 °C). 10% (w/w) PVA solution was obtained by dissolving PVA powders in de-ionised water and magnetically stirred at 90 °C for 5 h. Various amounts of HA powders (1, 3, 5, 7.5, and 10 wt%) were added into clear PVA solutions and ultrasonicated for 30 min before spinning.

**Co-Axial Pressurised Gyration:** A new co-axial pressurised gyration device was designed and made in the workshop (UCL, Department of Mechanical Engineering) to fabricate the PCL–PVA core-sheath fibers with HA nanoparticles on the surface. As shown in Figure 2, it has a detachable inner vessel (30 mm longitudinal diameter) and an outer vessel (60 mm diameter) connected to the DC motor and pressurised  $N_2$  gas is applied from the top. The motor is used to spin the vessel and the gas is used to pressurize the chamber and blow the polymer solutions to form core-sheath polymer fibers. The core part of the fiber was made through two inner nozzles (1 mm diameter) attached at the end of the inner vessel and extended to the circumference of the outer vessel which had two orifices (2 mm diameter) to form the sheath part of the fiber. The rotating speed of the spinning vessel could be maximized to 6000 rpm and the applied pressure could be maximized to  $3 \times 10^5$  Pa. In this work, 2 mL of PCL solution and 2 mL of PVA–HA solution was used as core and sheath materials, respectively, for each run to produce fibers. For each run, the fibers were spun at 6000 rpm rotating speed and  $1 \times 10^5$  Pa applied pressure at room temperature and relative humidity of 42%. The manufactured fibers were collected on an aluminium foil and rolled and cut into the fibrous scaffolds.

**Characterization: Viscosity and Surface Tension:** The viscosity and surface tension of the polymer solutions were measured by a viscometer (Brookfield, Harlow) and surface tensiometer (Kruss, Germany), respectively. For the viscosity measurement, the shear rate was varied between 0.132 and  $1.32\text{ s}^{-1}$  at room temperature.

**Optical Microscopy:** The morphology of the core-sheath fibers was observed using an optical microscope (Brunel microscopes). In order to confirm the core-sheath nature of formed fibers, rhodamine B (excitation wavelength 540 nm) and acriflavine (excitation wavelength 440 nm) were used for labeling and identifying individual sheath and core regions of the generated fibers.



**Scanning Electron Microscopy (SEM):** Fiber morphology and diameter evaluations were carried out by scanning electron microscope images obtained by an FE-SEM device (GAIA 3, Tescan Czech Republic). Fiber samples were coated with Au/Pd (EM ACE600, Leica, Germany) prior to analysis. The diameters of the produced fibers were determined using ImageJ (National Institutes of Health, US) software. For each sample, at least 100 fibers were randomly selected to quantify analysis.

**Fourier Transform Infrared (FTIR) Spectroscopy:** FTIR spectroscopy of different samples was carried out using a Bruker-Alpha machine with a monolithic crystal material attenuated total internal reflectance (ATR). The transmission spectra were recorded from 400–4000  $\text{cm}^{-1}$  wavelength with a scan resolution of 4  $\text{cm}^{-1}$ . The presence of different molecules in the core-sheath fibers were confirmed by FTIR spectroscopy.

**Water Contact Angle (WCA) of Fibrous Scaffolds:** The water contact angle ( $\theta$ ) of the scaffolds was measured in the surface tensiometer using the Wilhelmy plate method. The scaffolds were attached to known dimensions of the plate and gradually lifted out from the known surface tension of the liquid (water). The  $\theta$  was calculated from the following equation:  $\cos \theta = \frac{F}{L\sigma}$  where  $F$  is the measured force,  $L$  dimensions of plate, and  $\sigma$  is the surface tension of water.

**Swelling Ratios of the Fibrous Scaffolds:** The core-sheath fibrous scaffolds were cut into small pieces of equal weight. Swelling ratios were calculated by measuring the weight change ratios of samples before and after immersion in the de-ionised water at room temperature. Measurements were conducted in triplicate for each sample.

**Biological (In Vitro) Evaluation of Core-Sheath Fibers: In Vitro Cytotoxicity Assays:** Gyro-spun fiber samples obtained with different HA nanoparticles were divided into 200 mg portions, washed twice with phosphate buffer, soaked into 70% ethanol and then exposed to UV irradiation for the sterilization process. Samples were washed twice with phosphate buffer, dried, and placed into sealed vials containing 1 mL of culture media for 72 h.

SaOs-2 cells were used for the biological evaluations of core-sheath fiber samples. The cells were seeded at a concentration of  $1 \times 10^5$  cells per mL in tissue culture plate and cultured at 37 °C in 90% humidified air fed with 5%  $\text{CO}_2$ , and incubated overnight. The growth media consisted of DMEM supplemented with FBS by 10%. The cells were harvested from culture flask after reaching 80% confluency and seeded into 96 well plates at a density of  $1 \times 10^4$  cells per well and the cell media was replenished with the media interacted with the core-sheath fibers. The cells were allowed to proliferate for an additional 24 h incubation period. The cell viability was evaluated with both fluorescence-based LIVE/DEAD assay kit<sup>[67]</sup> and colorimetric MTT assays.<sup>[68]</sup>

For LIVE/DEAD analysis, cell media were replaced with 200  $\mu\text{L}$  phosphate buffer saline (PBS) solution containing 2 mM calcein AM and 4 mM ethidium homodimer-1, then the cells were allowed to interact with fluorescence dyes in the dark for 30 min. Representative images of green (live) and red (dead) cells were taken by a fluorescence microscope camera and color channels were merged with ImageJ software. Cell media was replaced with a 200  $\mu\text{L}$  fresh medium containing 20  $\mu\text{L}$  of MTT reagent (5 g  $\text{mL}^{-1}$ ) for the quantitative colorimetric metric assay. Cells were incubated in the dark for 4 h at 37 °C and the medium was discarded at the end of the trial. Blue formazan crystals formed as a result of mitochondrial activity were dissolved by isopropanol-HCl solution (0.04 M HCl in absolute isopropanol). 100  $\mu\text{L}$  solution from each well was pipetted into 96-well analyzing plate and relative cell viabilities against the negative control group were calculated by the absorbance spectra at 570 nm wavelength.

**Cell Observation with SEM:** The observation of adhered cells on the surfaces of fibers was evaluated by a SEM on the 4th day of the culture. Fiber scaffolds used in cell culture were washed twice with warm PBS and Saos-2 cells were fixed with 2.5% (v/v) glutaraldehyde in 0.1 M PBS (pH 7.4) for 30 min at ambient conditions. The samples were washed again twice with 0.1 M PBS (pH 7.4) for the removal of unreacted glutaraldehyde. The cells were dehydrated with varying concentrations of ethanol (30, 50, 70, 90, and 100% (v/v)) for 5 min in each solution. After dehydration of cells, a drop of hexamethylidisilazane was placed on each sample and the samples were dried in air at room temperature.

**Alkaline Phosphatase Activity:** Alkaline phosphatase (ALP) activity of Saos-2 cells on the 7th and 14th days was evaluated with an alkaline phos-

phatase assay kit according to the manufacturer's protocol. Briefly, cells cultured on fiber scaffolds were washed with cold PBS and homogenized on ice. Samples were centrifugated at 14 000 rpm for 15 min and supernatants were collected for analysis. 5 mM p-nitrophenyl phosphate (pNPP) solution was used as a phosphatase substrate for the samples and allowed to incubate in the dark for 60 min. The absorbance values were measured at 405 nm and activities were calculated with the equation obtained from the calibration curve plotted with standard samples.

## Acknowledgements

The authors are grateful to the UK Engineering & Physical Sciences Research Council (EPSRC) for funding pressurised gyration forming research at the University College London to the value of  $\approx$ £1.5 million (Grants EP/L023059/1, EP/N034228/1, and EP/S016872/1). Hacettepe University is thanked for the collaboration and resourcing the cellular work. The authors would also like to thank Mr Peter Kelly and Mr Angelo Delbusso of the UCL Mechanical Engineering workshop who advised on the design and making of the core-sheath fiber making devices.

## Conflict of Interest

The authors declare no conflict of interest.

## Data Availability Statement

Data available upon a reasonable request from the author.

## Keywords

bone, core-sheath, fiber, pressurized gyration, scaffold, tissue engineering

Received: April 27, 2021

Revised: June 21, 2021

Published online:

- [1] J. S. Jíří Nedoma, I. Hlavacek, J. Danek, T. Dostálová, *Mathematical and Computational Methods and Algorithms in Biomechanics: Human Skeletal Systems*, John Wiley & Sons, **2011**, 12, Introduction to the Anatomy of Skeletal System 9.
- [2] J. Henkel, M. A. Woodruff, D. R. Epari, R. Steck, V. Glatt, I. C. Dickinson, P. F. M. Choong, M. A. Schuetz, D. W. Huttmacher, *Bone Res.* **2013**, 1, 216.
- [3] A. Salhotra, H. N. Shah, B. Levi, M. T. Longaker, *Nat. Rev. Mol. Cell Bio.* **2020**, 21, 696.
- [4] C. G. Finkemeier, *J. Bone Jt. Surg.* **2002**, 84, 454.
- [5] E. P. E. Silva, B. Huang, J. V. Helaehil, P. R. Nalesso, L. Bagne, M. A. de Oliveira, G. C. Albiazetti, A. Aldalbah, M. El-Newehy, M. J. B.-D. Santamaria-Jr, *Manufacturing* **2021**, 4, 190.
- [6] M. Dang, L. Saunders, X. Niu, Y. Fan, P. X. Ma, *Bone Res.* **2018**, 6, 25.
- [7] F.-Y. Hsu, H.-W. Hsu, Y.-u.-H. Chang, J.-L. Yu, L.-R. Rau, S.-W. Tsai, *Mater. Sci. Eng., C* **2018**, 89, 346.
- [8] J.-Y. Park, J.-H. Lee, C.-H. Kim, Y.-J. Kim, *RSC Adv.* **2018**, 8, 34359.
- [9] N. A. Pattanashetti, D. D. Achari, A. I. Torvi, R. V. Doddamani, M. Y. Kariduraganavar, *Materialia* **2020**, 12, 100826.
- [10] R. Langer, J. Vacanti, *Science* **1993**, 260, 920.
- [11] G. L. Koons, M. Diba, A. G. Mikos, *Nat. Rev. Mater.* **2020**, 5, 584.
- [12] H. Liu, M. Lin, X. Liu, Y. Zhang, Y. Luo, Y. Pang, H. Chen, D. Zhu, X. Zhong, S. Ma, Y. Zhao, Q. Yang, X. Zhang, *Bioact. Mater.* **2020**, 5, 844.

- [13] D. K. Patel, S. D. Dutta, J. Hexiu, K. Ganguly, K.i-T. Lim, *Int. J. Biol. Macromol.* **2020**, *162*, 1429.
- [14] C. Wang, J. Lai, K. Li, S. Zhu, B. Lu, J. Liu, Y. Tang, Y. Wei, *Bioact. Mater.* **2021**, *6*, 137.
- [15] N. F. Huang, S. Patel, R. G. Thakar, J. Wu, B. S. Hsiao, B. Chu, R. J. Lee, S. Li, *Nano Lett.* **2006**, *6*, 537.
- [16] K. Huang, G. Liu, Z. Gu, J. Wu, *Chin. Chem. Lett.* **2020**, *31*, 3190.
- [17] Y. Zhou, Z. Gu, J. Liu, K. Huang, G. Liu, J. Wu, *Carbohydr. Polym.* **2020**, *230*, 115640.
- [18] Z. Bao, Z. Gu, J. Xu, M. Zhao, G. Liu, J. Wu, *Chem. Eng. J.* **2020**, *396*, 125353.
- [19] S. Mahalingam, R. Matharu, S. Homer-Vanniasinkam, M. Edirisinghe, *Appl. Phys. Rev.* **2020**, *7*, 041302.
- [20] H. Samadian, H. Mobasheri, M. Azami, R. Faridi-Majidi, *Sci. Rep.* **2020**, *10*, 14853.
- [21] G.u Cheng, C. Yin, H.u Tu, S. Jiang, Q. Wang, X. Zhou, X. Xing, C. Xie, X. Shi, Y. Du, H. Deng, Z. Li, *ACS Nano* **2019**, *13*, 6372.
- [22] J. R. García, A. Y. Clark, A. J. García, *J. Biomed. Mater. Res., Part A* **2016**, *104*, 1845.
- [23] W. Song, X. Yu, D. C. Markel, T. Shi, W. Ren, *Biofabrication* **2013**, *5*, 035006.
- [24] X. Cheng, G.u Cheng, X. Xing, C. Yin, Y. Cheng, X. Zhou, S. Jiang, F. Tao, H. Deng, Z. Li, *J. Controlled Release* **2020**, *319*, 234.
- [25] N. Manhas, K. Balasubramanian, P. Prajith, P. Rule, S. Nimje, *RSC Adv.* **2015**, *5*, 23999.
- [26] H. Wu, J. Fan, C. - C. Chu, J. Wu, *J. Mater. Sci.: Mater. Med.* **2010**, *21*, 3207.
- [27] R. Johnson, Y. Ding, N. Nagiah, E. Monnet, W. Tan, *Mater. Sci. Eng., C* **2019**, *97*, 1.
- [28] A. F. Martins, S. P. Facchi, P. C. F. Da Câmara, S. E. A. Camargo, C. H. R. Camargo, K. C. Popat, M. J. Kipper, *J. Colloid Interface Sci.* **2018**, *525*, 21.
- [29] N. Nagiah, R. Johnson, R. Anderson, W. Elliott, W. Tan, *Langmuir* **2015**, *31*, 12993.
- [30] Q. Pan, C. Gao, Y. Wang, Y. Wang, C. Mao, Q. Wang, S. N. Economidou, D. Douroumis, F. Wen, L. P. J. B.-D. Tan, *Manufacturing* **2020**, *3*, 396.
- [31] H. Saniee, S. Mousavi, *Polymer* **2020**, *196*, 122467.
- [32] V. Chopra, J. Thomas, A. Sharma, V. Panwar, S. Kaushik, S. Sharma, K. Porwal, C. Kulkarni, S. Rajput, H. Singh, K. Jagavelu, N. Chattopadhyay, D. Ghosh, *ACS Biomater. Sci. Eng.* **2020**, *6*, 6710.
- [33] N. Bahrami, M. Bayat, A. Ai, M. Khanmohammadi, J. Ai, A. Ahmadi, M. Salehi, S. Ebrahimi-Barough, A. Goodarzi, R. Karimi, A. Moahamadnia, A. Rahimi, *Arch Neurosci.* **2018**, *5*, e74267.
- [34] Y. Yang, Y. Cheng, F. Deng, L. Shen, Z. Zhao, S. Peng, C. Shuai, *Bio-Design and Manufacturing* **2021**, *4*, 452.
- [35] I.n-G.u Kang, J. Kim, S. Park, H.-E.e Kim, C. -M. Han, *Macromol. Biosci.* **2020**, *20*, 2000136.
- [36] S. Suvarnapathaki, X. Wu, D. Lantigua, M. A. Nguyen, G. Camci-Unal, *Macromol. Biosci.* **2020**, *20*, 2000176.
- [37] S. Mahalingam, S. Homer-Vanniasinkam, M. Edirisinghe, *Mater. Des.* **2019**, *178*, 107846.
- [38] S. Mahalingam, S. G. Huo, S. Homer-Vanniasinkam, M. Edirisinghe, *Polymers* **2020**, *12*, 1709.
- [39] X. Gao, S. Han, R. Zhang, G. Liu, J. Wu, *J. Mater. Chem. B* **2019**, *7*, 7075.
- [40] S. Mahalingam, M. Edirisinghe, *Macromol. Rapid Commun.* **2013**, *34*, 1134.
- [41] A. Amir, H. Porwal, S. Mahalingam, X. Wu, T. Wu, B. Chen, T. A. Tabish, M. Edirisinghe, *Compos. Sci. Technol.* **2020**, *197*, 108214.
- [42] P. L. Heseltine, J. Hosken, C. Agboh, D. Farrar, S. Homer-Vanniasinkam, M. Edirisinghe, *Macromol. Mater. Eng.* **2019**, *304*, 1800577.
- [43] M. Hermosín-Reyes, A. M. Gañán-Calvo, L. B. Modesto-López, *J. Aerosol Sci.* **2019**, *137*, 105429.
- [44] J. M. Montanero, A. M. Gañán-Calvo, *Rep. Prog. Phys.* **2020**, *83*, 097001.
- [45] M. Gultekinoglu, Ş. Öztürk, B. Chen, M. Edirisinghe, K. Ulubayram, *Eur. Polym. J.* **2019**, *121*, 109297.
- [46] A. M. Gañán-Calvo, C. Ferrera, J. M. Montanero, *J. Fluid Mech.* **2011**, *670*, 427.
- [47] R. Singh, S. Khan, S. M. Basu, M. Chauhan, N. Sarviya, J. Giri, *ACS Appl. Bio Mater.* **2019**, *2*, 5340.
- [48] Y. Han, C.e Shi, F. Cui, Q. Chen, Y. Tao, Y. Li, *Polymer* **2020**, *122806*, 204.
- [49] J. Matulevicius, L. Kliucininkas, T. Prasauskas, D. Buivydiene, D. Martuzevicius, *J. Aerosol Sci.* **2016**, *92*, 27.
- [50] Z. -C. Yao, J. -C. Wang, Z. Ahmad, J. -S. Li, M. -W. Chang, *Mater. Sci. Eng., C* **2019**, *97*, 776.
- [51] N. V. Bhat, M. M. Nate, M. B. Kurup, V. A. Bambole, S. Sabharwal, *Nucl. Instrum. Methods Phys. Res., Sect. B* **2005**, *237*, 585.
- [52] J. Lee, T. Isobe, M. Senna, *J. Colloid Interface Sci.* **1996**, *177*, 490.
- [53] S. Suganthi, S. Vignesh, J. Kalyana Sundar, V. Raj, *Appl. Water Sci.* **2020**, *10*.
- [54] M. Manoj, D. Mangalaraj, N. Ponpandian, C. Viswanathan, *RSC Adv.* **2015**, *5*, 48705.
- [55] A. Satpathy, A. Pal, S. Sengupta, A. Das, M.d. M. Hasan, I. Ratha, A. Barui, S. Bodhak, *J. Indian Inst. Sci.* **2019**, *99*, 289.
- [56] C. Mouro, M. Simões, I. C. Gouveia, *Adv. Polym. Tech.* **2019**, *2019*, 9859506.
- [57] F. Sharifi, S. Irani, M. Zandi, M. Soleimani, S. M. Atyabi, *Prog. Biomater.* **2016**, *5*, 213.
- [58] X. Luo, Z. Guo, P. He, T. Chen, L. Li, S. Ding, H. Li, *Int. J. Biol. Macromol.* **2018**, *113*, 476.
- [59] K. Seo, M. Kim, D. H. Kim, in *Surface Energy* (Ed: M. Aliofkhaezrai), IntechOpen, London, UK **2015**.
- [60] C. Gao, M. Yao, C. Shuai, P. Feng, S. Peng, *Bio-Design and Manufacturing* **2020**, *3*, 307.
- [61] K. Kim, D. Dean, A. Lu, A. G. Mikos, J. P. Fisher, *Acta Biomater.* **2011**, *7*, 1249.
- [62] G. Mendonça, D. B. S. Mendonça, L. G. P. Simões, A. L. Araújo, E. R. Leite, W. R. Duarte, F. J. L. Aragão, L. F. Cooper, *Biomaterials* **2009**, *30*, 4053.
- [63] J.-H.o Kim, D.-K. Kim, O.k J. Lee, H. W. Ju, J. M. Lee, B.o M.i Moon, H. J. Park, D. W. Kim, J. H.o Lee, C. H. Park, *Int. J. Biol. Macromol.* **2016**, *82*, 160.
- [64] C. Bayram, M. Demirebilek, N. Çalişkan, M. E. Demirebilek, E. B. Denkbcş, *J. Biomed. Nanotechnol.* **2012**, *8*, 482.
- [65] J. J. Li, E. S. Gil, R. S. Hayden, C. Li, S.-I. Roohani-Esfahani, D. L. Kaplan, H. Zreiqat, *Biomacromolecules* **2013**, *14*, 2179.
- [66] X. Li, Y. Yuan, L. Liu, Y.-S. Leung, Y. Chen, Y. Guo, Y. Chai, Y. J. B.-D. Chen, *Manufacturing* **2020**, *3*, 15.
- [67] F. Yi, D. A. Lavan, *Macromol. Biosci.* **2008**, *8*, 803.
- [68] Z. Kroneková, M. Mikulec, N.ž Petrenčíková, E. Paulovičová, L. Paulovičová, V. Jančinová, R. Nosál, P. S. Reddy, G. D. Shimoga, D. Chorvát, J. Kronek, *Macromol. Biosci.* **2016**, *16*, 1200.